Supplemental Material

1. Supplementary Methods

Expression analysis of virus-injected mice

Immunohistochemistry was performed as described (Shimshek et al., 2005). Mice were anesthetized and intracardially perfused with PBS and 4% PFA in PBS. Brains were isolated, fixed in cold 4% PFA in PBS for 1-3 h, cut into 70-100 um slices on a vibratome and treated for double-labeling with primary (Cre, polyclonal, BAbCo, 1:3000; NeuN, monoclonal, DAKO, 1:1000) and secondary (FITC-coupled goat anti-rabbit, Cy3-coupled goat anti-mouse, 1:200, Jackson Antibodies) antibodies. Slices were cover-slipped with Vectashield (Vector) and analyzed with a fluorescence Zeiss microscope and Leica SP2 confocal microscope. To determine the fraction of infected GCs, the number of cells positive for both Cre- and NeuN were counted and presented as a fraction of the total number of NeuN-positive cells within the GC layer.

Western Blots of OB protein were performed as described (Shimshek et al., 2005). Mice brains were removed, and OBs were isolated. Total protein was prepared, and immunoblots were performed as described. Antibodies used were against GluA2 (1:800, monoclonal; Chemicon), GluN1 (1:600, polyclonal, Chemicon), GluA1 (1:2000, polyclonal, Chemicon), β-actin (1:40,000, monoclonal; Sigma) as an internal standard, and secondary peroxidase-coupled goat anti-rabbit and goat anti-mouse antibodies (Vector, 1:15,000). Immunoreactivity was detected with ECLplus (Amersham), and immunoblots were scanned and quantitatively analyzed with ImageJ. Data are presented as mean ± SEM. Statistical significance was evaluated by two-tailed, unpaired student-*t* test.

Immunohistochemistry of GluA1 and GluA2 in the OB

Immunohistochemistry of GluA1 and GluA2 in C57BL6: Mice were anesthetized and intracardially perfused with PBS and 4% PFA in PBS.

Brains were isolated, fixed in cold 4% PFA in PBS for 1-3 h. They were permeated with 10% sucrose in PBS and 10% polyvinyl pyrrolidone (PVP) for 4 hrs at 4^0C followed by 20% sucrose in PBS and 10% PVP for 4 hrs at 4^0C and 30% sucrose in PBS and 10% PVP for overnight at 4^0C and cut into 10 µm slices in a cryochamber. Before treated with anitibodies, sections were warmed to 37^0C for 15 min. Double-labeling antibody staining was done with primary (Rabbit polyclonal GluA1, Chemicon International, Hofheim, Germany, 1:20, Rabbit polyclonal GluA2, Chemicon International, Hofheim, Germany, 1:20) and secondary (Alexa-coupled goat anti-rabbit 567, 1:300 and Alexa-coupled goat anti-rabbit 488, 1:300, Molecular Probes) antibodies. Slices were cover-slipped with Vectashield (Vector) and analyzed with a fluorescence Zeiss microscope and Leica SP2 confocal microscope.

Immunohistochemistry of GluA2 and Cre in $GluA2^{\Delta GCL}$: Coronal or sagittal 70-100 µm thick vibratome slices were used as described (Shimshek et al., 2006) with primary antibodies (Cre, polyclonal, BAbCo, 1:3000; Rabbit polyclonal GluA2, Chemicon International, Hofheim, Germany), and secondary anti-rabbit antibodies. Secondary anti-rabbit antibodies coupled to horseradish-peroxidase and biotinylated secondary antibodies (each 1:600) and ABC kit were used (Vector Laboratories, Peterborough, United Kingdom). Slices were stained with 3-3' diaminobenzidine (DAB) (Sigma Taufkirchen, Germany), mounted on slides and air-dried. DAB-developed slices were coversliped with eu-kitt (O. Kindler, Freiburg, Germany) and analyzed with a Axiovert 100 Zeiss microscope (Carl Zeiss MicroImaging, Göttingen, Germany).

Analysis of granule cell morphology

The morphology of the neurons can be assessed by overexpression of membrane-bound GFP (De Paola et al., 2003). mGFP was subcloned into the pAM plasmid (see above) to yield pAM-mGFP. We took advantage of the high coinfection rate when using AAV particles delivering different genes to achieve simultaneous expression of Cre recombinase and mGFP.

Tuning of the injection parameters allowed visualization of individual Cre-expressing and non-expressing granule cells in the same slice (see Supplementary Fig. S3). Three-week old *GluA2*^{2lox} mice were injected simultaneously with equal amounts of AAV-Cre and AAV1/2-mGFP particles. An incubation time of 6 weeks was chosen to match that of the behavioral experiments. The brains were isolated after transcardial perfusion, fixed in cold 4% PFA in PBS for 1-3 h, cut into 70µm slices on a vibratome and treated with primary (Cre, polyclonal, BAbCo, 1:3000) and secondary (Alexa647-coupled goat anti-rabbit, 1:1000, Molecular Probes) antibodies. Slices were cover-slipped with Vectashield (Vector) and analyzed with a Leica SP2 confocal microscope. Two independent observers analyzed morphology of 9 Cre expressing and 9 non-expressing granule cells. The entire dendritic tree was classified into primary, secondary, tertiary and quaternary dendrites for counting the number of spines in the dendritic branches. All spines with a neck and clear spine head were counted. The number of spines per dendritic length is presented as mean ± SD.

Recording synaptic Ca^{2+} transients in GCs

Somatic whole-cell patch-clamp recordings were performed using an EPC-9 amplifier (HEKA, Lambrecht, Germany) following previously published procedures (Egger et al., 2003). The intracellular solution contained [mM]: 130 K-methylsulfate, 10 HEPES, 4 MgCl2, 4 Na2ATP, 0.4 NaGTP, 10 NaPhosphocreatine, 2 ascorbate, 0.1 OGB-1 (Invitrogen, Carlsbad, USA), at pH 7.2. The extracellular artificial cerebrospinal fluid was bubbled with carbogen and contained [mM]: 125 NaCl, 26 NaHCO3, 1.25 NaH2PO4, 20 Glucose, 2.5 KCl, 1 MgCl2 and 2 CaCl2. All experiments were performed at room temperature (~ 21° C).

GCs were identified by their morphological appearance and the shape of their current evoked APs and firing patterns (Egger et al., 2003). GluA2-depleted GCs were identified by somatic KO fluorescence arising from simultaneous expression of Cre recombinase and KO (Tang et al.,

2009). The average input resistance of the investigated GCs was on the order of 1 GΩ and their resting potential was ranging from -80 to -70 mV, similar to our previous data (Egger et al. 2003, Egger 2008). Because of the strong presence of LVA calcium channels in GCs (Egger et al. 2003; Pinato & Midtgaard, 2003), GCs were generally held within the range given above. Leaky GCs that required more than 30 pA of holding current were rejected. Mitral cell synaptic input onto GCs was generated as described previously via extracellular glomerular stimulation (Egger et al., 2005; Egger, 2008). A monopolar wire electrode connected to a stimulator (STG4004; Multi Channel Systems, Reutlingen, Germany; stimulus duration 100 us, maximal amplitude 800 uA) was placed into a glomerulus, and active spines were identified as described earlier on (Egger et al. 2005).

Imaging was performed on an Olympus Fluoview system (Olympus Europe, Hamburg, Germany), with two-photon excitation at 800 nm provided by a Ti:Sapphire solid-state laser system (Mai Tai, Spectraphysics, Mountain View, CA, USA). The microscope was equipped with a 60x Nikon fluor water immersion objective (NA 1.0; Nikon Instruments, Amstelveen, The Netherlands). Infected cells were identified via their fluorescence at 750 nm excitation prior to patching. Kusabira orange was barely excited at the wavelength of 800 nm used for Ca^{2+} imaging; thus the apparent F0 of OGB-1 was not increased in the labeled cells.

Fluorescence transients were imaged in line-scan mode (temporal resolution 2 ms) at different locations along the apical dendrite of GCs and within its spines, typically within the external plexiform layer. Transients were recorded at a stimulus repetition rate of 0.1 Hz.

Imaging and electrophysiological data were analyzed with custom software written in Igor (WaveMetrics, Lake Oswego, OR, USA). To measure changes in calcium, fluorescence was collected while scanning in a line that intersected the region(s) of interest. Fluorescence F(t) was then averaged over the region(s) of interest. Baseline fluorescence F_0 was

measured for 50 ms before the stimulus, and ΔF/F was calculated as $(\Delta F/F)(t) = (F(t) - F_0)/F_0$. Evoked and spontaneous synaptic signals were identified as described before (Egger et al. 2003, 2005).

Analysis of recurrent inhibition recorded *in vivo*

Sweeps of 5 s duration were collected with an intersweep interval of at least 5 s. All available traces for 20 evoked APs were averaged after APs were clipped (Supplementary Fig. S4A); AP positions were calculated by differentiating the membrane potential trace and generously blanking out regions ±3.75 ms around any point for which the absolute value of the differential was above 2% of its maximal value. Blanked out regions were then filled in by linear interpolation; for display purposes, all AP clipping was restricted to times > 340 ms after trial begin.

As the prominent subthreshold oscillation (Margrie & Schaefer, 2003, Cang & Isaacson, 2003, Schaefer et al., 2006) masks any AP-induced small membrane potential changes, a "blank" trace was measured as follows: APs were clipped as above, and traces were aligned to the peak of the respiration plethysmograph signal between 1500 and 1900 ms after trial onset (Supplementary Fig. S4B1), and both the respiration and the voltage signal were averaged (Supplementary Fig. S4B2). The resultant averaged Vm was then aligned to the averaged Vm based on the (averaged) respiration recordings (Supplementary Fig. S4B2 bottom and S4A3 bottom) and subtracted from it (Supplementary Fig. S4C). The resultant difference trace was normalized to a membrane potential baseline measured between 1500 and 2000 ms after trial onset. This time period was late enough not to interfere with the recurrent IPSP. The membrane potential for the difference before normalization was -0.3±0.3 mV (n=29 mean±SEM). The baseline before the onset of stimulation (0-100 ms) appeared too short for reliable normalization, although normalizing to this baseline nevertheless did not change the comparison of recurrent IPSP amplitude between control and *GluA2*$^{\Delta FB}$.

The resultant normalized difference trace was then inspected for residual subthreshold oscillations: The entire trace between 350 and 2000 ms after trial onset (green line in Supplementary Fig. S5A1) was autocorrelated, and the ratio between the first peak (between 200 and 1500 ms, blue line in Supplementary Fig. S5A3) and the central peak (t=0 ms) relative to the intermediate trough was measured (Supplementary Fig. S5A3). Supplementary Fig S5A1 and A2 show two examples of the subtraction procedure working efficiently (A1) and when it reduced the amplitude of the oscillation but could not abolish it entirely (A2). Top traces show averaged membrane potential before (gray) and after (black) subtraction. Supplementary Fig. S5A3 indicates the points in the autocorrelogram used for amplitude and thus "remaining oscillatory component (ROC)" estimation (ROC=1st off center peak / central peak). Cells were excluded based on a maximal ROC threshold, which was usually set to 0.6 (based on visual inspection of the individual traces). This resulted in five cells being excluded. Other exclusion criteria did not qualitatively alter our findings (see below).

The amplitude of recurrent inhibition was measured as the minimal voltage between 350 ms and 650 ms (Supplementary Fig. S4D1, blue). Other measures used were the integral from after AP discharge until 2000ms after trial begin (blue in Supplementary Fig. S4D3) and the amplitude of a fitted alpha function starting at 322 ms [$f(t)=A\ e^{-0.3(x-322ms)/t1}\ (1-e^{-(x-322ms)/t2})$].

All results were insensitive against the ROC cutoff: in all cases recurrent inhibition was substantially stronger for *GluA2*$^{\Delta FB}$ animals (Supplementary Fig. S5B), no matter what fraction of cells were excluded based on the remaining oscillatory nature of the membrane potential difference (threshold varying from 0.4 (n=4 vs. n=10) to 1 (n=9 vs. n=20)).

2. Supplementary References

De Paola, V., Arber, S., and Caroni, P. (2003). AMPA receptors regulate dynamic equilibrium of presynaptic terminals in mature hippocampal networks. Nat Neurosci *6*, 491-500.

Cang,J. and Isaacson,J.S. (2003). In vivo whole-cell recording of odor-evoked synaptic transmission in the rat olfactory bulb. J Neurosci 23, 4108-4116.

Egger,V., Svoboda,K., and Mainen,Z.F. (2003). Mechanisms of lateral inhibition in the olfactory bulb: efficiency and modulation of spike-evoked calcium influx into granule cells. J Neurosci 23, 7551-7558.

Egger,V., Svoboda,K., and Mainen,Z.F. (2005). Dendrodendritic synaptic signals in olfactory bulb granule cells: local spine boost and global low-threshold spike. J Neurosci 25, 3521-3530.

Egger V. (2008). Synaptic sodium spikes trigger long-lasting depolarizations and slow calcium entry in rat olfactory bulb granule cells. Eur J Neurosci. 27, 2066-75.

Margrie,T.W., Meyer,A.H., Caputi,A., Monyer,H., Hasan,M.T., Schaefer,A.T., Denk,W., and Brecht,M. (2003). Targeted whole-cell recordings in the mammalian brain in vivo. Neuron 39, 911-918.

Pinato,G. and Midtgaard,J. (2003). Regulation of granule cell excitability by a low-threshold calcium spike in turtle olfactory bulb. J Neurophysiol 90, 3341-3351.

Schaefer,A.T., Angelo,K., Spors,H., and Margrie,T.W. (2006). Neuronal oscillations enhance stimulus discrimination by ensuring action potential precision. PLoS Biol 4, e163.

Shimshek, D. R., Bus, T., Grinevich, V., Single, F. N., Mack, V., Sprengel, R., Spergel, D. J., and Seeburg, P. H. (2006). Impaired reproductive behavior by lack of GluA2 containing AMPA receptors but not of NMDA receptors in hypothalamic and septal neurons. Mol Endocrinol *20*, 219-231.

Tang,W., Ehrlich,I., Wolff,S.B., Michalski,A.M., Wolfl,S., Hasan,M.T., Luthi,A., and Sprengel,R. (2009). Faithful expression of multiple proteins via 2A-peptide self-processing: a versatile and reliable method for manipulating brain circuits. J Neurosci 29, 8621-8629.

3. Supplementary Figures

Figure S1: AAV-Cre expression restricted to the OB.
A. Magnified view of the marked region of the section shown in Fig. 1. No Cre immunoreactivity could be detected outside the OB (e.g. in piriform cortex).
B. Region encompassing anterior olfactory nucleus (AON), and lateral olfactory tract (LOT).

Figure S2: Immunolocalization of GluA1 and GluA2 in the OB.
A. Expression of GluA2 (green) and GluA1 (red) in the OB of C57BL6 mice (Immunofluorescence). Overlay reveals extensive coexpression of the two subunits (yellow). Expression is higher in the glomerular layer compared to the other layers.
B. Expression of Cre recombinase and GluA2 in the OB of *GluA2*^{2lox} mice (DAB-stain). Left panel shows entire OB with only the right side expressing Cre recombinase. Corresponding set of sections shows a reduced expression of GluA2 only on the right side. Right panel shows magnified view of another representative example. GluA2 expression is reduced in the granule cell and external plexiform layers in the presence of Cre recombinase.

Figure S3: Morphology of granule cells lacking GluA2.
Morphology of GCs in the OB of *GluA2*^{2lox} mice visualized by mGFP expression. A small fraction of granule cells was infected with AAV-Cre and AAV-mGFP, allowing comparison of the morphology in cells expressing Cre recombinase with unperturbed cells.
A. Cre-positive granule cell (red nucleus, anti-Cre antibody stain) labeled with mGFP (green fluroescence). The entire dendritic tree is captured. (scale bar 25 µm).
B. Granule cell visualized with mGFP not expressing Cre recombinase, taken from the same tissue as the cell shown in A. (scale bar 20 µm).

C. The number of spines per dendrite length was not significantly different (scale bar 10 µm, Cre-expressing cells: 0.29±0.09, n=9, control cells: 0.3±0.09, n=9, mean±SD; p=0.8, student-*t* test).

Figure S4: Measurement and quantification of recurrent inhibition *in vivo*.
A. Twenty APs are elicited by intracellular current injection (top trace) triggered on a plethysmograph recording of the respiratory rhythm (bottom traces). In the resultant membrane potential recordings (A1) APs are clipped (A2) and traces are averaged (A3).
B. To obtain a baseline recording, traces are aligned to the respiration during the period indicated by the blue bar. Note the slight desynchronization due to the naturally variable breathing rhythm (dotted line). (B2) Traces are averaged and re-aligned with respect to the averaged respiration recording (compare blue circle in A3 and B2).
C. Aligned background recording is subtracted from the averaged evoked response to virtually eliminate background oscillations.
D. Traces are normalized to a baseline late during the recording (green bar) and recurrent inhibition is measured as (D1) the voltage minimum during the period indicated by the blue bar; as (D2) the integral (dark blue shading), or as (D3) the amplitude of a fitted alpha function. The time course of the alpha function was determined from the averaged waveform of all recurrent IPSPs (the average of the averaged control and averaged *GluA2*$^{\Delta FB}$ waveform) leaving its amplitude as the only variable. Scale bars are 20 mV and 1000 ms (A-C) and 2 mV and 500 ms (D).

Figure S5: Quality and impact of the background oscillation subtraction.
A1. Example of the averaged membrane potential before (gray, middle trace) and after (black, top trace) background subtraction. (Bottom graph) autocorrelation function before (black) and after (gray) background subtraction for the time period indicated in green. A2. Same as A1 but for a different cell where background subtraction could not be performed as efficiently. Note the strong oscillatory component in the autocorrelation

even after background subtraction. (A3) Quantification of the remaining oscillatory component (ROC).

B. Recurrent inhibition as a function of the ROC. Cells were excluded if ROC exceeded the indicated threshold. Note that independent of the exclusion criterion, inhibition is substantially increased for *GluA2*$^{\Delta FB}$ (red) compared to control (black).

Figure S6: Stimulus protocol specifically elicits recurrent inhibition

A. Representative example traces of patch-clamp recording from mitral cells in OB slices of C57BL6 mice. Control (black), in presence of D-AP5 (green), in presence of BAPTA-AM (red) and in presence of GABAzine (blue).

B. Quantification of the experiments shown in A. D-AP5 (n=10 cells), BAPTA-AM (n=12 cells) and GABAzine (n=13 cells).

C. Mitral cells were filled with 50 µM Alexa during patch-recordings and their morphology was documented after the experiment. Two representations, arrowheads show the dissected axon end with typical terminal swelling. (Scale bar 50 µm).

Figure S7: Behavioral paradigm and motivational parameters

A. Scheme of the experimental design. After a light beam (red line) is broken, an odor is presented; a water reward is given at the end of an S+ (rewarded) odor. Odor discrimination time is the time after odor onset at which responses to S+ and S- odors differ significantly (see Methods). Bar depicts time line of individual trial. Odor onset is 500 ms after trial initiation.

B. Intertrial interval as a measure of motivation. No significant difference was observed in activity levels of *GluA2*$^{\Delta GCL}$ (17.8±1.8 s, n=11) and control mice (23.7±3.5 s, n=13) for simple odors (p=0.2, student-*t* test) and similar odor mixtures (*GluA2*$^{\Delta GCL}$, 22.7±3.1 s, n=11, control mice, 20.3±2.2 s, n=13 p=0.5, student-*t* test, compare to Abraham et al, 2004).

C. As in B but using *GluN1*$^{\Delta GCL}$ mice. No difference observed in activity levels of *GluN1*$^{\Delta GCL}$ (30.7±3.6 s, n=10) and control mice (28.6±5.4 s, n=9) for simple odors (p=0.8, student-*t* test) and similar odor mixtures (*GluN1*$^{\Delta GCL}$, 29.1±3.9 s, n=10, Control mice, 27.2±5.1 s, n=9, p=0.8, student-*t* test).

Figure S8: Kinetics and pharmacology of spontaneous EPSPs in GCs.

A. *In vitro* recordings of *s*pontaneous EPSPs (sEPSPs) from control, ΔGluA2 and ΔGluN1 GCs. sEPSPs decayed significantly faster in ΔGluN1 GCs compared to GCs of control animals (34.2±2.2 ms, n=17 vs 19.2±3.2, n=9, p<0.002), but remained unaltered in ΔGluA2 GCs (37.3±3.7 ms, n=9, p=0.5). The amplitude of sEPSPs in ΔGluN1 GCs was increased in comparison to control (6.6 ± 2.0 mV, n = 9 cells versus 3.6 ± 1.3 mV, n = 10 cells, P = 0.002, Mann-Whitney-test; GluA2-deleted cells: 4.2 ± 1.6 mV, n = 9 cells). This increase in amplitude may reflect redistribution or subtle rearrangements in the synaptic glutamate receptor composition not detected by immunoblotting (Fig. 6C).

B. Pharmacological properties of sEPSPs in GCs. (B1) Examples of spontaneous sEPSPs before (top) and after (bottom) application of 25 µM APV to the bath. (B2) Quantification of sEPSP decay kinetics from experiments as in B1. In control animals sEPSPs were significantly sped up by application of APV (τ_{APV}=25.0±2.7 ms vs τ_{NoDrug}=32.6±3.9 ms, n=7, p<0.005) whereas in ΔGluN1 no change was observed (τ_{APV}=24.7±4.1 ms vs τ_{NoDrug}=23.0±4.4 ms, n=3, p=0.3). The speeding up of the EPSP kinetics with APV was significantly stronger in control animals (ratio NoDrug/APV=1.31±0.06 for control vs 0.93±0.04 for ΔGluN1; p<0.002).

[G] Supplemental Text and Figures

Click here to download high resolution image

Figure S1

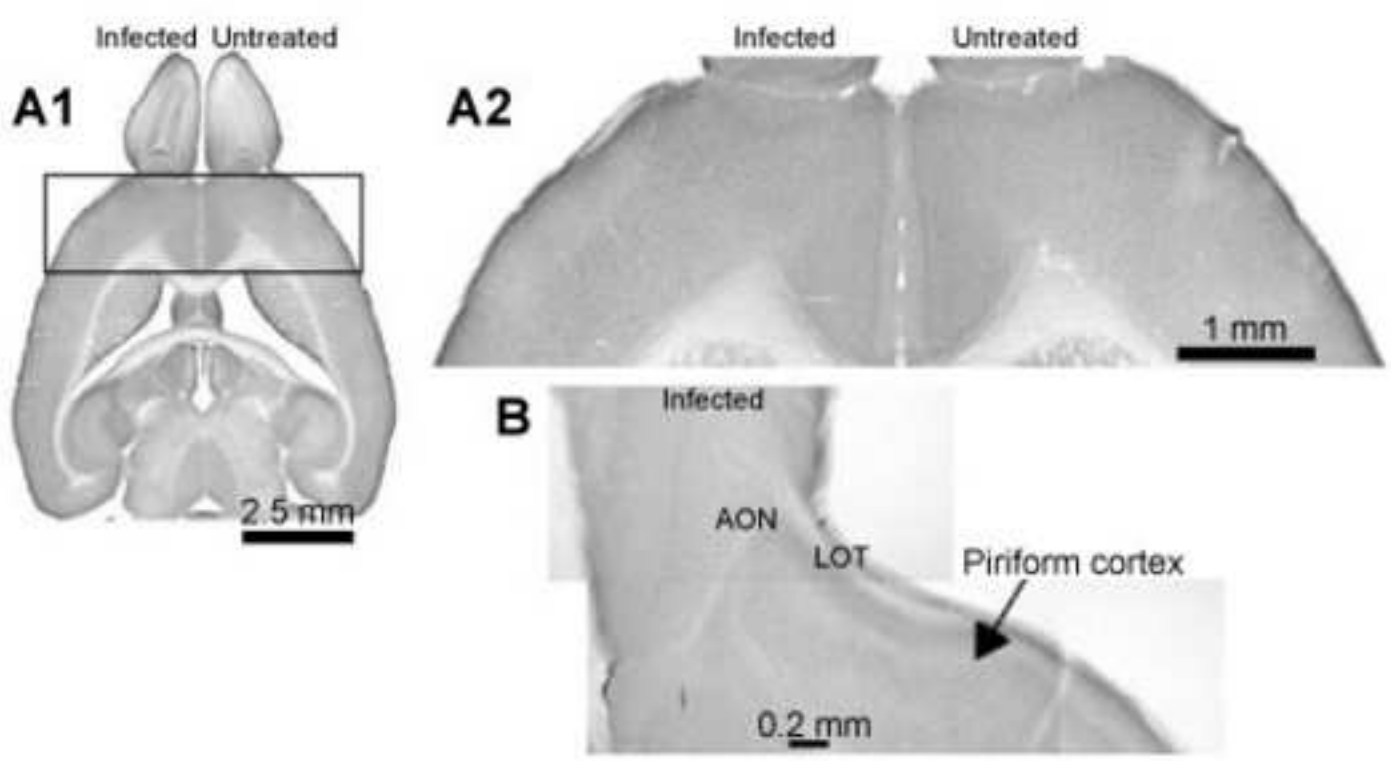

[G] Supplemental Text and Figures

Click here to download high resolution image

Figure S2

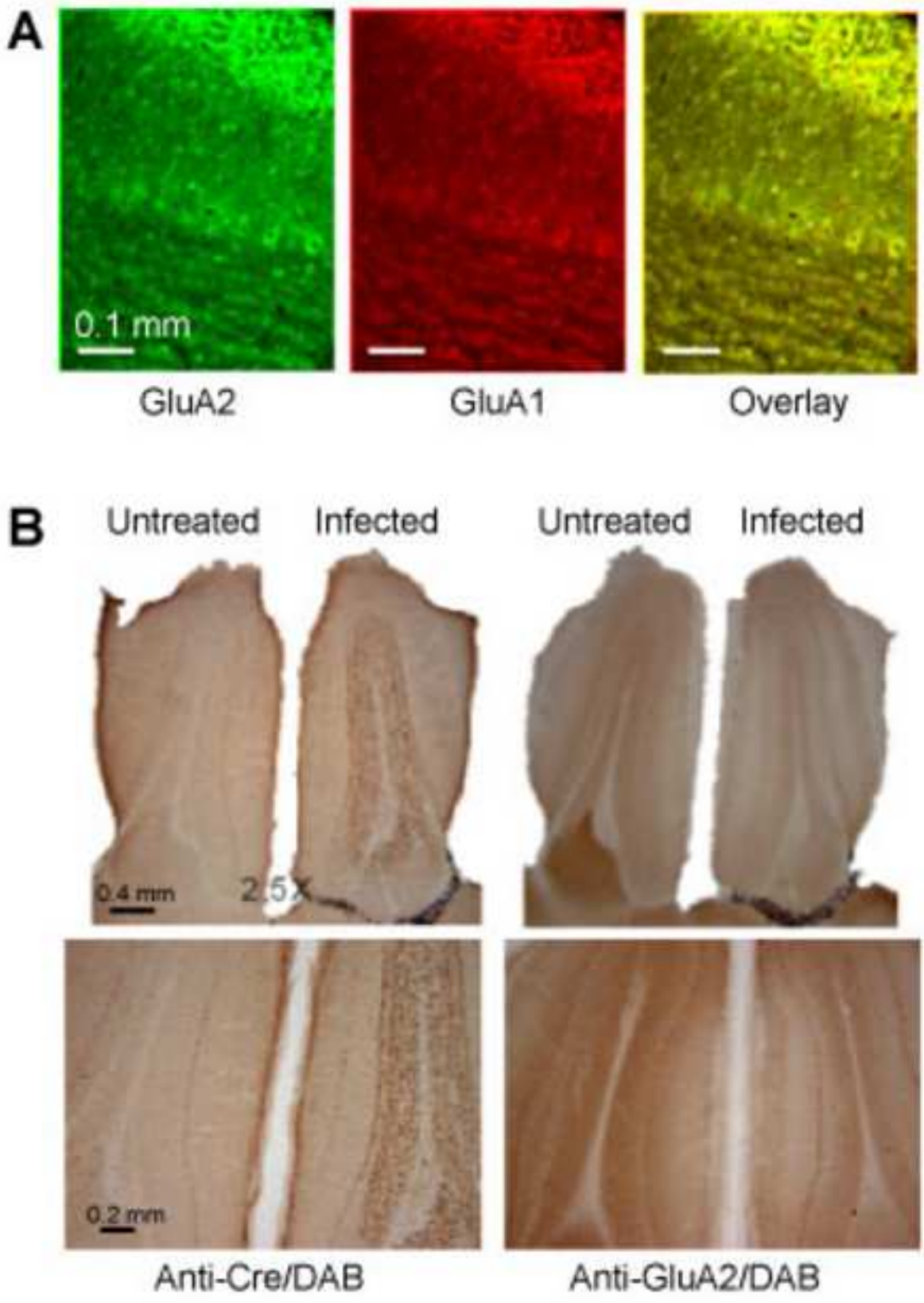

[G] Supplemental Text and Figures

Click here to download high resolution image

Figure S3

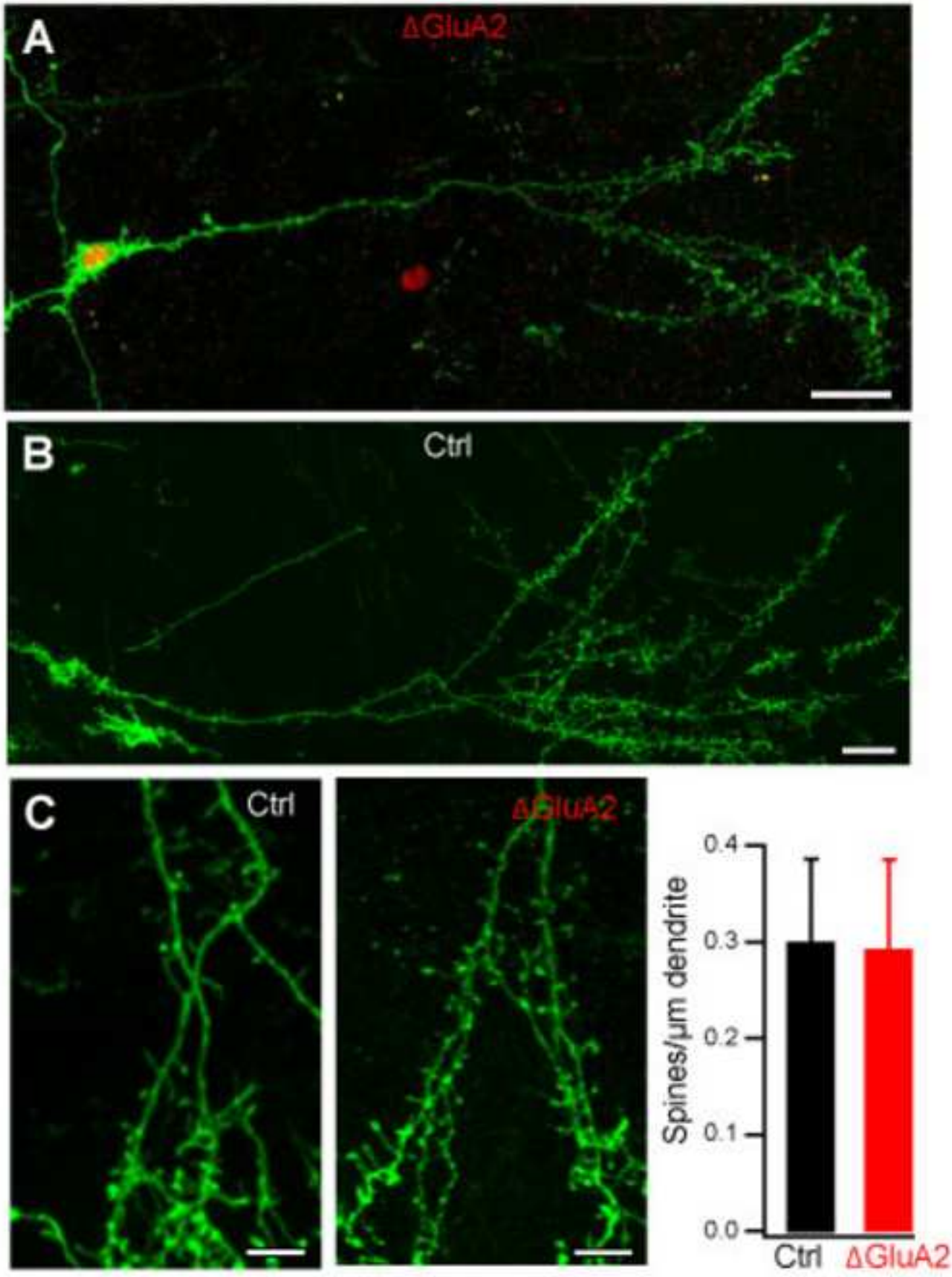

[G] Supplemental Text and Figures

Click here to download high resolution image

Figure S4

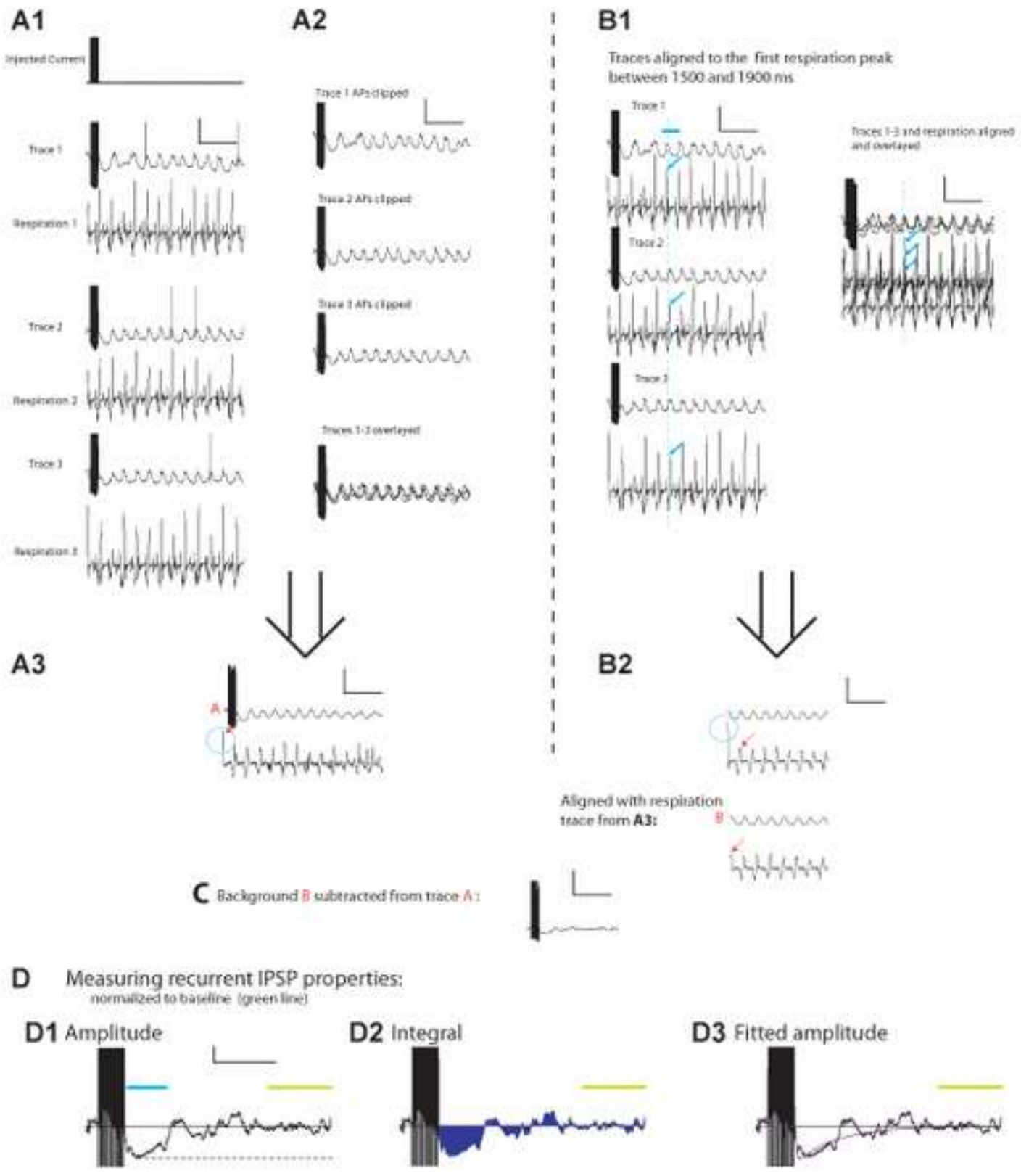

Figure S5

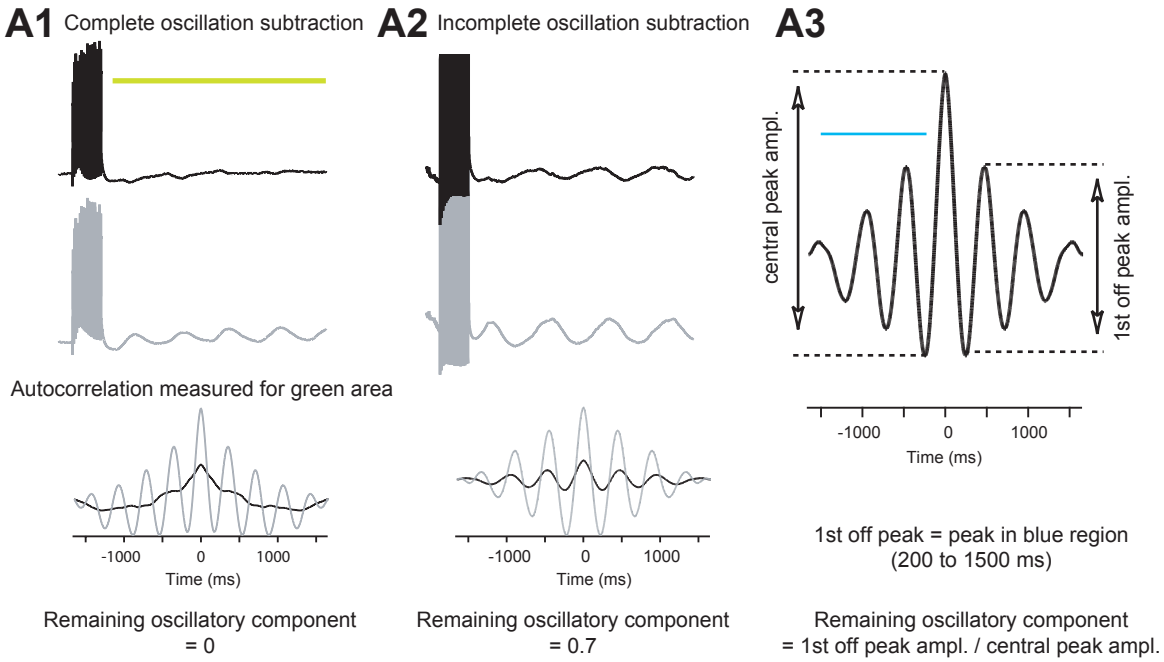
A1
Complete oscillation subtraction
A2
Incomplete oscillation subtraction
A3
central peak ampl.
1st off peak ampl.
-1000
0
1000
Time (ms)
Autocorrelation measured for green area
-1000
0
1000
Time (ms)
-1000
0
1000
Time (ms)
1st off peak = peak in blue region
(200 to 1500 ms)
Remaining oscillatory component
= 0
Remaining oscillatory component
= 0.7
Remaining oscillatory component
= 1st off peak ampl. / central peak ampl.

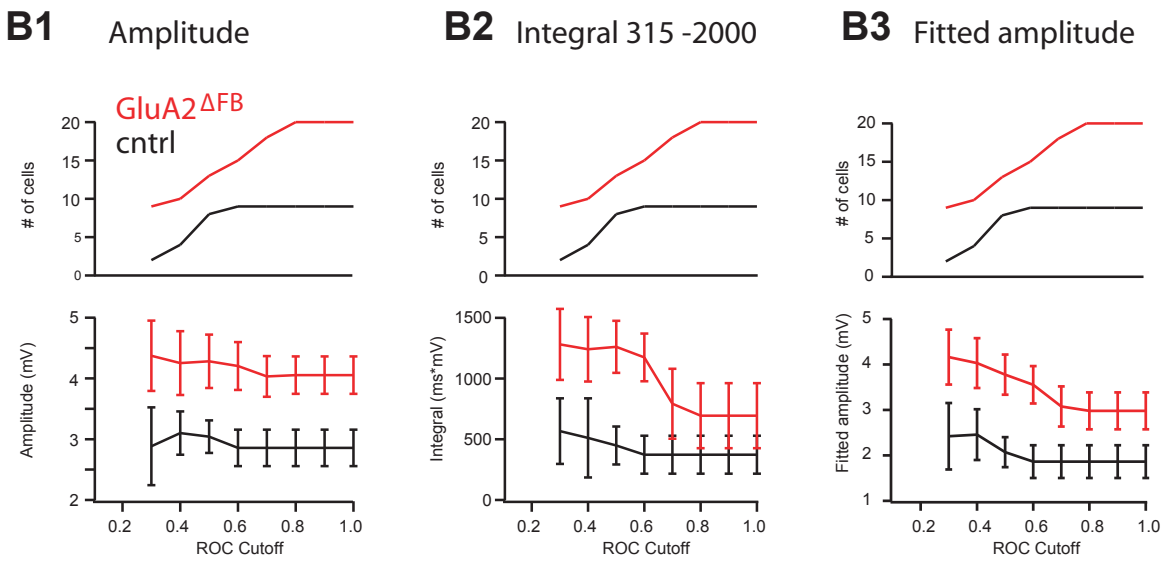
B1
Amplitude
B2
Integral 315 -2000
B3
Fitted amplitude
GluA2ΔFB
cntrl
# of cells
Amplitude (mV)
Integral (ms*mV)
Fitted amplitude (mV)
ROC Cutoff
ROC Cutoff
ROC Cutoff

Figure S6

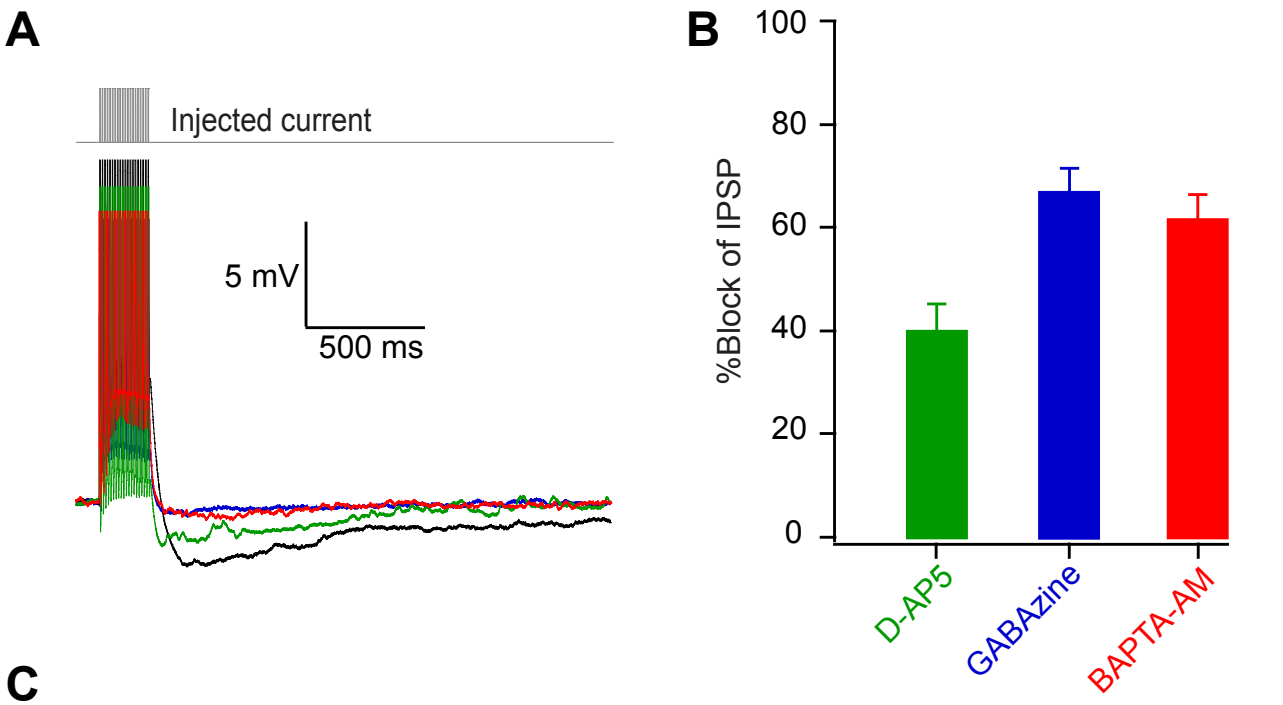
A
Injected current
5 mV
500 ms
B
100
80
60
40
20
0
%Block of IPSP
D-AP5
GABAzine
BAPTA-AM

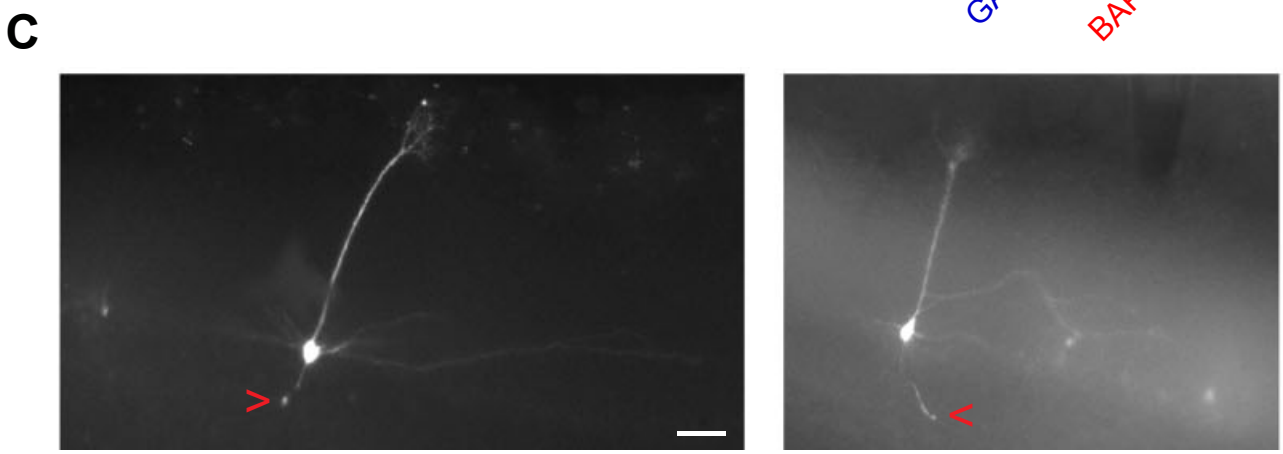
C

Figure S7

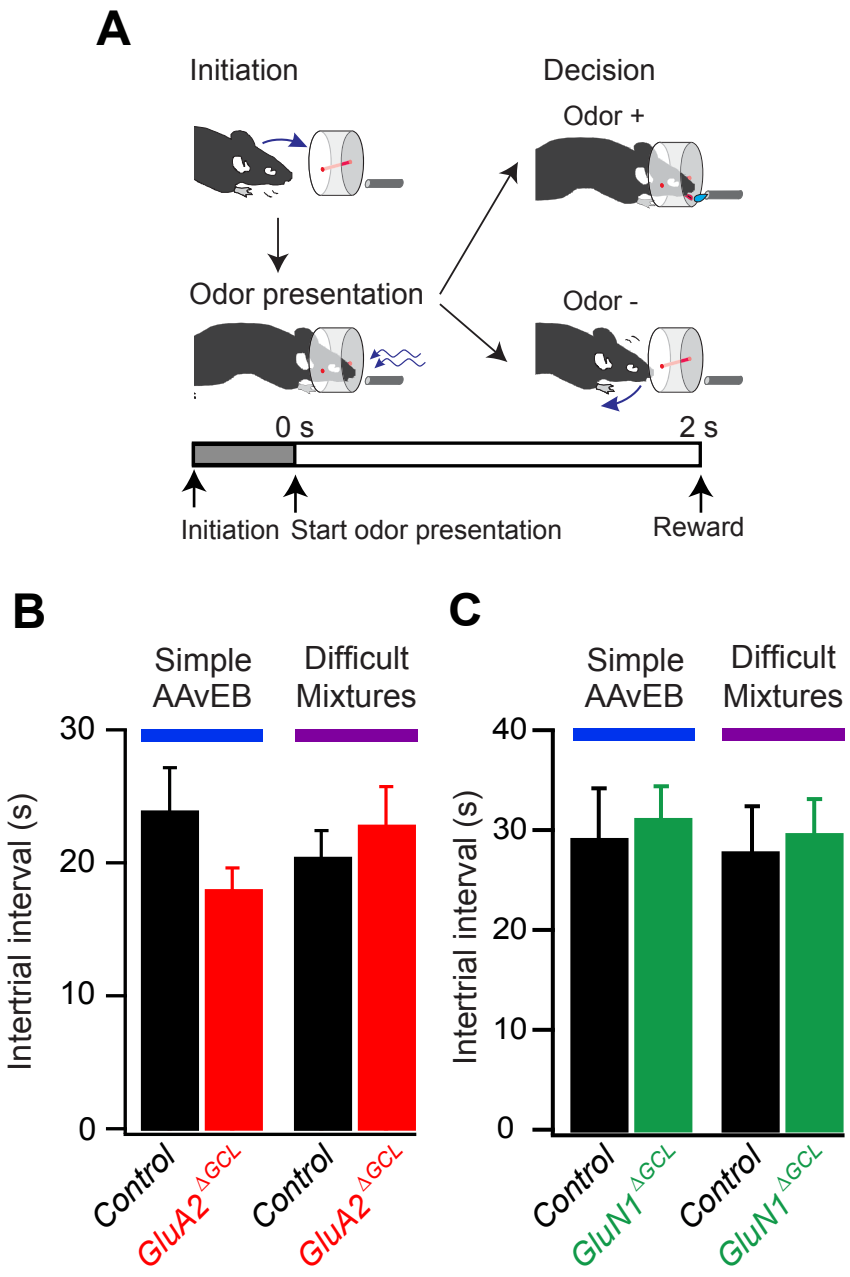
A
Initiation
Decision
Odor +
Odor presentation
Odor -
0 s
2 s
Initiation
Start odor presentation
Reward
B
Simple AAvEB
Difficult Mixtures
Intertrial interval (s)
30
20
10
0
Control
GluA2ΔGCL
Control
GluA2ΔGCL
C
Simple AAvEB
Difficult Mixtures
Intertrial interval (s)
40
30
20
10
0
Control
GluN1ΔGCL
Control
GluN1ΔGCL

Figure S8

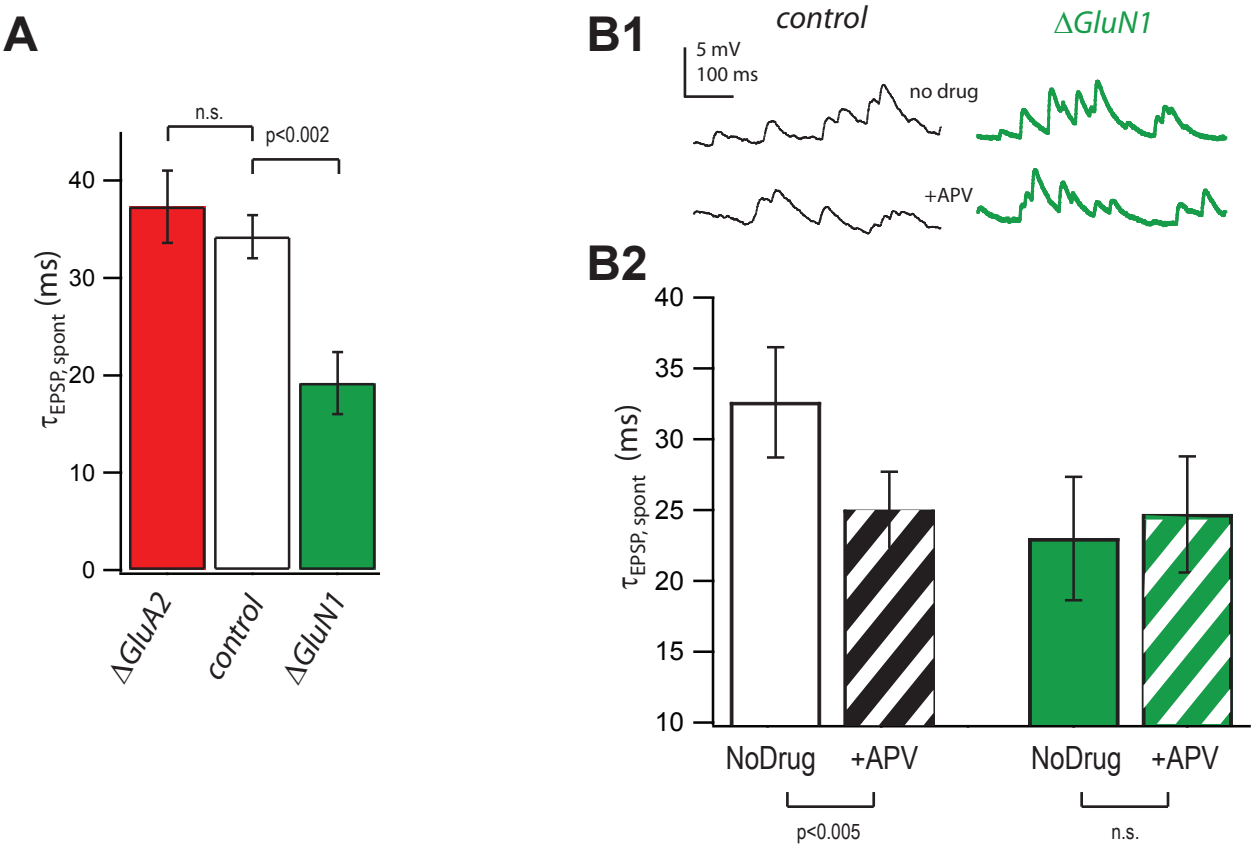
A
n.s.
p<0.002
40
30
20
10
0
τEPSP, spont (ms)
ΔGluA2
control
ΔGluN1
B1
control
ΔGluN1
5 mV
100 ms
no drug
+APV
B2
40
35
30
25
20
15
10
τEPSP, spont (ms)
NoDrug
+APV
NoDrug
+APV
p<0.005
n.s.